This is the accepted version of the following article:

Xiaodong Ji*, Yuhao Cheng, Tongseng Leong, Yao Cui. Seismic behavior and strength capacity of steel coupling beam-SRC wall joints. Engineering Structures, 2019, 201: 109820.

which has been published in final form at [Link to final article]

Seismic behavior and strength capacity of steel coupling beam-to-SRC wall joints

Xiaodong Ji[1], Yuhao Cheng[2], Tongseng Leong[3], Yao Cui[4]

[1]*Associate professor, Key Laboratory of Civil Engineering Safety and Durability of China Education Ministry, Department of Civil Engineering, Tsinghua University, Beijing 100084, China*

[2]*Graduate student, Beijing Engineering Research Center of Steel and Concrete Composite Structures, Department of Civil Engineering, Tsinghua University, Beijing 100084, China*

[3]*Graduate student, Department of Civil Engineering, Tsinghua University, Beijing 100084, China*

[4]*Associate professor, State Key Laboratory of Coastal and Offshore Engineering, Faculty of Infrastructure Engineering, Dalian University of Technology, Dalian, Liaoning 116024, China*

Abstract: A hybrid coupled wall system, where steel coupling beams couple steel reinforced concrete (SRC) walls in series, has been recognized as an alternative to reinforced concrete (RC) coupled wall systems for enhanced seismic performance of high-rise buildings. A key issue of this system is seismic design of steel coupling beam-to-SRC wall joints. This paper presents a series of full-scale tests to investigate the cyclic behavior and strength capacity of the steel coupling beam-to-SRC wall joints, where a steel beam was rigidly connected to an encased steel column in wall boundary using a fully welded connection detail. The steel beam-to-SRC wall joints failed in panel shear mode, characterized by yielding of the steel web panel and joint transverse reinforcement, and crisscrossed-diagonal cracking and crushing of joint panel concrete. A design model for calculating the nominal strength of the steel beam-to-SRC wall joint is presented. The accuracy of the design model was verified against the collected test data and additional finite element (FE) analysis. The experimental tests and FE analysis also identified that severe vertical cracks might developed along the inner side of wall boundary element, due to horizontally tensile forces by the steel beam flange. Increased amount of horizontally distributed rebar is recommended

Please cite this article as: Xiaodong Ji*, Yuhao Cheng, Tongseng Leong, Yao Cui. Seismic behavior and strength capacity of steel coupling beam-SRC wall joints. Engineering Structures, 2019, 201: 109820.

to be assigned in around the join region, in order to control such unwanted damage. In addition, the test results of one specimen demonstrated that properly designed beam-to-wall joint remained slightly damaged when the steel coupling beam fully developed its plastic rotation.

Keywords: steel coupling beams; steel reinforced concrete (SRC) walls; hybrid coupled wall system; steel coupling beam-to-SRC wall joint; seismic behavior; strength capacity; design model

1. Introduction

Reinforced concrete (RC) coupled walls, which consist of wall piers connected with RC coupling beams throughout their height, are often used as the structural system for high-rise buildings due to their recognized lateral strength and stiffness benefits. In recent years, the steel coupling beams or replaceable steel coupling beams have been identified as a promising alternative to the traditional RC coupling beams (e.g., [1-8]), because they can provide more stable cyclic response, larger plastic rotation and superior energy dissipation capacity when subjected to severe ground motions. On the other hand, the steel reinforced concrete (SRC) walls, which consists of the structural steel column embedded in the boundary elements of RC walls, have seen increasing use in high-rise buildings in the regions of high seismicity. The addition of encased steel columns can increase the flexural and shear strength, and deformation capacity of structural walls [9-12]. Therefore, a combination of the steel coupling beams and SRC walls is expected to form an attractive hybrid coupled wall system for enhanced seismic performance of high-rise buildings.

A key issue for design of the hybrid coupled wall system is how the steel coupling beam can be effectively jointed to wall piers. Based on past extensive research (e.g., Shahrooz et al. [13], Harries et al. [1], and Park and Yun [14], etc.), the design of steel coupling beam-to-RC wall joints has been matured. Design provisions, including the strength formulas and detailing requirements for such joints, have been specified in the design codes, e.g., the AISC 341-10 [15]. However, seismic design method for the steel coupling beam-to-SRC wall joint has yet to be fully developed, due to a lack of experimental data. As such, the current codes do not provide detailed design provisions on the steel coupling beam-to-SRC wall joints.

Recently, an increased attention has been given to the study of seismic behavior of the steel coupling beam-to-SRC wall joints. For example, Song [16] conducted experimental tests on six steel coupling beam-to-SRC wall subassembly specimens where the steel coupling beams were connected to the encased steel columns using a fully welded connection. Among those specimens five were controlled by yielding of steel coupling beams, while one was intentionally designed with the "strong beam-weak joint" mechanism and the strength was governed by the joint. Wu et al. [17] presented experimental tests on four specimens where the steel coupling beams were connected to the encased steel columns using an end-plate connection with high-strength bolts. All specimens failed due to the fracture of end plates in the connection. Li et al. [18] reported experimental tests on steel coupling beam-to-wall joints, where two specimens having encased long steel column behaved similarly to steel coupling beam-to-SRC wall joints. For these specimens, the steel coupling beams were connected to the encased steel columns using a welded connection and additional extended stiffeners. Upon to date, the experimental data for strength capacity of steel coupling beam-to-SRC wall joints has yet been limited, particularly for those joints using fully welded connection details which are commonly used in practice. Therefore, there is a clear need to further accumulate fundamental test data for development of design recommendations of steel coupling beam-to-SRC wall joints.

Although a theoretical model has been proposed for calculating the nominal strength of steel coupling beam-to-SRC wall joints [19], design equations and detailing recommendations have not yet been well validated. In this study, three full-scale steel coupling beam-to-SRC wall assembly specimens were tested to investigate the cyclic behavior and strength capacity of the joints. Using the test data and additional finite element (FE) analysis, the objective of this paper is to develop and validate the strength design model for the steel coupling beam-to-SRC wall joints. Another objective of this paper is to quantify the extent of possible seismic damage and the post-quake reparability of the steel beam-to-SRC wall joint, if it is capacity designed following the "strong joint-weak coupling beam" philosophy. The second section presents the experimental program. The test results are described in the third section. The fourth section presents the design model for calculating the nominal strength of joints, and calibrates this model using test data. Finally, the sophisticated FE model is developed using ABAQUS program for further validating the mechanism and accuracy of the design model of joint strength.

2. Experimental program

2.1. Specimen design

The full-scale test specimen represented a coupling beam-wall subassembly in mid-stories of an 11-story high-rise building. The prototype structure was located in Beijing, and used a shear wall-frame interacting system. The peak ground acceleration of the design basis earthquake (DBE, with a probability of exceedance of 10% in 50 years) for the site is 0.2 g. The structure was designed according to the modern Chinese design codes, including the Chinese Code for Seismic Design of Buildings (GB 50011-2010) [20] and Chinese Technical Specification for Concrete Structures of Tall Buildings (JGJ 3-2010) [21]. Linear response spectrum analysis was performed to determine the inter-story drifts and force demands of structural components that are used for structural design. In the response spectrum analysis, the steel coupling beam-to-wall pier connection was assumed to be rigid by neglecting the local deformation of joints. When the prototype structure is subjected to the DBE motions, the steel coupling beams are expected to yield, while the coupling beam-to-wall joints are designed to remain elastic by proportioning their strength higher than the overstrength capacity of the coupling beams.

The subassembly consisted of one story of wall pier and the coupling beams. A total of three specimens were designed and fabricated. Fig. 1 shows the geometric dimensions and reinforcement details of the specimens. In each test specimen, one structural wall pier was connected to two steel coupling beams at its two edges. A steel column was encased in one boundary element of the wall and the steel coupling beam was rigidly jointed to the encased steel column using fully welded connection details, representing the steel coupling beam-to-SRC wall joint. Another wall boundary element did not consist of the full-length encased steel column, and the steel coupling beam was directly embedded in the wall pier or jointed with the wall through a short embedded steel column, representing the steel coupling beam-to-RC wall joint. A foundation beam and top beam were casted together with the wall pier. The encased steel column and vertical reinforcement were securely anchored with those beams. The foundation beam was capacity designed to ensure that it was damage free during the loading. The flexural and shear strengthes of the foundation beam calculated per the Chinese Code for Design of Concrete Structures (GB 50010-2010) [22] were approximately 1.7 times of its maximum bending moment and shear force demands. The steel beams and steel columns were fabricated in factory and shipped to the laboratory. Assembling reinforcement and pouring concrete were conducted in the laboratory, and the specimens were casted in an upright position. The concrete was supplied by the industry, and the design strength grade of concrete was C45 (nominal cubic compressive strength $f_{cu,n}$ = 45 MPa).

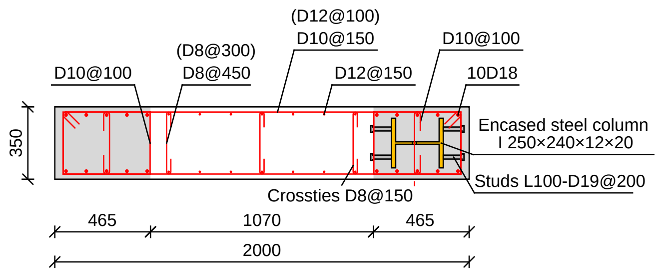

(a) Cross section of wall piers

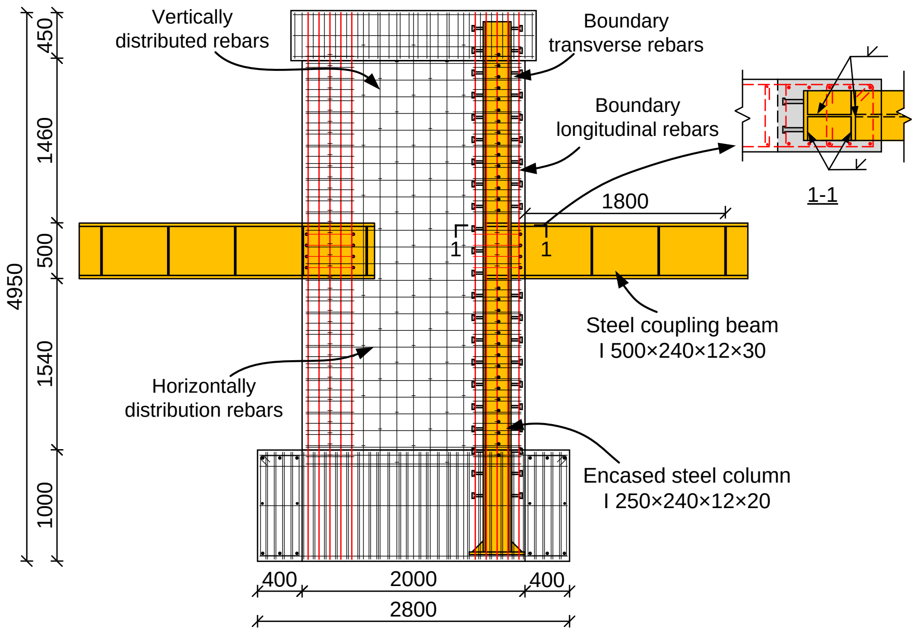

(b) Elevation drawing of steel reinforcement for SRC1

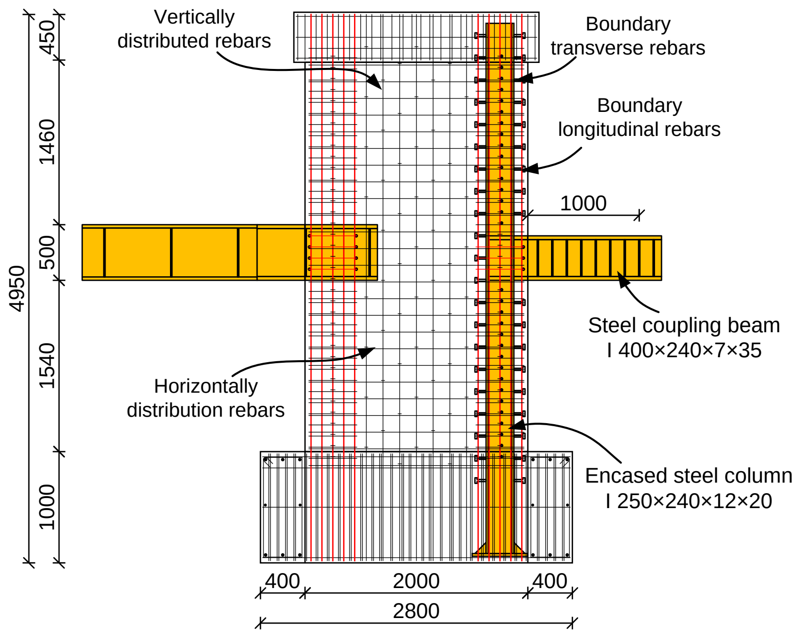

(c) Elevation drawing of steel reinforcement for SRC2

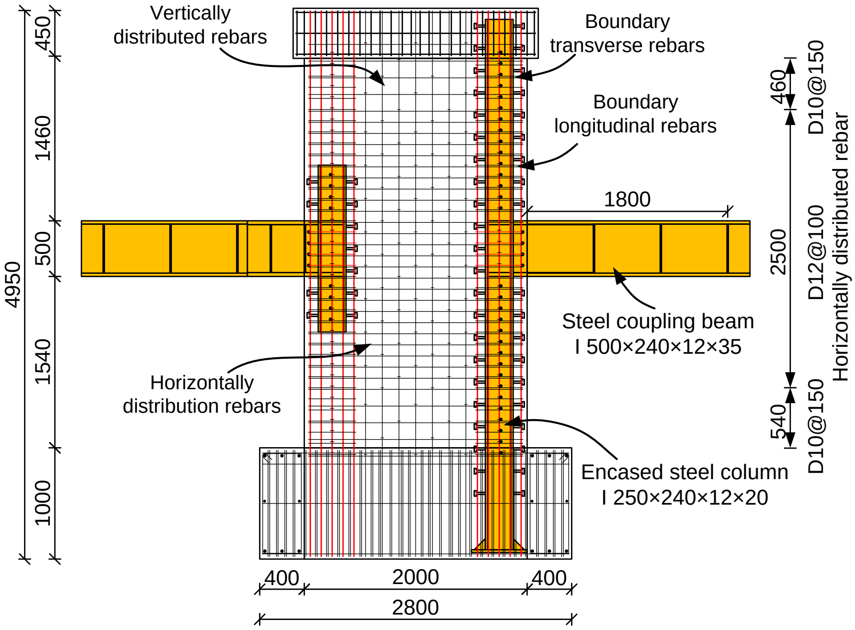

(d) Elevation drawing of steel reinforcement for SRC3

Fig. 1. Geometric dimensions and reinforcement details of specimens (unit: mm).

Each specimen was tested twice, first on the steel coupling beam-to-RC wall joint and then on the steel coupling beam-to-SRC wall joint. As the wall pier had relatively large size, the damage to one joint nearly had no influence on the behavior of the other joint at the opposite edge. Therefore, the tests made full use of one specimen to produce more data. This paper presents the tests on the steel coupling beam-to-SRC wall joints, while those tests on the steel coupling beam-to-RC wall joints are not described as they are out of the scope of this paper.

The three specimens were labelled as SRC1, SRC2 and SRC3. Specimens SRC1 and SRC3 were intentionally designed with strong coupling beams whose strength exceeded the beam-to-wall joint strength capacity. As such, the failure occurred in the beam-to-wall joint, and the maximum strength capacity of the joint could be obtained from the experimental tests. Specimen SRC2 was designed with a relatively smaller steel coupling beam, and the joint was designed with a nominal strength exceeding the overstrength capacity of the steel coupling beam. The SRC2 test was used to identify the extent of possible seismic damage and the reparability of the steel beam-to-SRC wall joint that was capacity designed and well detailed.

2.2. Wall piers

The geometric dimensions of wall piers for all specimens were identical. The clear height of the wall pier was 2500 mm. The wall section had a depth of 2000 mm and a thickness of 350 mm. The boundary elements that extend for 465 mm from the wall face were designed for the wall piers. A total of ten D18 (diameter of 18 mm) steel rebar was used as longitudinal reinforcement for each boundary element, corresponding to a 1.56% reinforcement ratio (the ratio of gross cross-sectional area of boundary longitudinal rebar to that of the boundary element). The boundary transverse reinforcement consisted of D10 steel rebar fabricated as rectangular hoops and supplementary crossties with a vertical spacing of 100 mm. The volumetric transverse reinforcement ratio of the boundary elements was equal to 1.1%. The boundary elements and reinforcing details of the wall piers satisfied the requirements for ordinary boundary elements of structural walls specified in the Chinese code GB 50011-2010 [20].

The vertically distributed reinforcement in the wall web comprised D12 rebar at a spacing of 150 mm, corresponding to a 0.45% reinforcement ratio. The horizontally distributed reinforcement comprised D10 rebar at a spacing of 150 mm, corresponding to a 0.31% reinforcement ratio. It is noted that an increased amount of horizontally distributed rebar (i.e., D12 rebar at a spacing of 100 mm) was assigned for specimen SRC3 in the region from 1000 mm below the joint to 1000 mm above the joint, as shown in Fig. 1(d). As will be explained later, it was designed to control the vertical cracks developed along the inner side of wall boundary element and to prevent the possible separating between the wall web and boundary element.

The encased steel column had a section of I 250 × 240 × 12 × 20 (sectional depth × width × web thickness × flange thickness, unit in mm). The reinforcement ratio of encase steel (the ratio of the cross-sectional area of encased steel column to that of the boundary element) was 7.4%. As shown in Fig. 1, two lines of shear studs were welded along each flange of the steel column with a vertical spacing of 200 mm, in order to develop the composite action between encased structural steel and surrounding concrete. The studs had an overall length of 100 mm, a stud diameter of 19 mm and a stud head diameter of 32 mm.

2.3. Steel coupling beams

As shown in Fig. 1, the cantilever steel beams in the test specimens were used to represent the half-span of coupling beams, and the vertical loading point of the cantilever beams corresponded to the inflection point of the coupling beams. The steel beams were built-up I-shapes. The flanges and webs were connected by complete-joint-penetration (CJP) groove welds.

Table 1 summaries the design parameters of the coupling beams. The cross sections of the coupling beams were I 500 × 240 × 12 × 30 for specimen SRC1 and I 500 × 240 × 12 × 35 for specimen SRC3. The distance a from the vertical loading point of cantilever beam to the wall face was 1.8 m for specimens SRC1 and SRC3. The length ratio of steel coupling beams, $2a/(M_{pb}/V_{pb})$, was equal to 2.98 and 2.52 for SRC1 and SRC3, respectively, where M_{pb} and V_{pb} denote the plastic flexural strength and plastic shear strength of the steel beam section. As the length ratio of the steel coupling beams was greater than 1.6, their nominal inelastic strength V_{nb} shall be governed by flexure and calculated by $V_{nb} = M_{pb}/a$. The value of V_{nb} was equal to 772 and 892 kN for steel beams in specimens SRC1 and SRC3, respectively. Note that the steel beams of the two specimens were designed with a strength higher than the nominal strength capacity of beam-to-wall joint (see Table 1), and they were thus expected to remain elastic during the testing. The intermediate stiffeners of steel beams of SRC1 and SRC3 were 12 mm thick and they were placed with a distance of 600 mm.

The cross-section of the steel coupling beam of specimen SRC2 was I 400 × 240 × 7 × 35. The width-to-thickness ratios for both beam flanges and web satisfied the requirements for link beams specified in the AISC 341-10 provisions [15]. The distance a from the vertical loading point of cantilever beam to the wall face was 1000 mm. The length ratio $2a/(M_{pb}/V_{pb})$ of the steel coupling beam of specimen SRC2 was equal to 0.81, and this beam was expected to yield primarily in shear. The plastic shear strength $V_{pb} = 0.6f_yA_w$ was equal to 473 kN, where f_y denotes the yield strength of beam steel web and A_w denotes the cross-sectional area of beam web. The intermediate web stiffeners were provided to delay premature web buckling and ensure adequate plastic rotation capacity of the steel beam. The stiffeners were 10 mm thick, and they were fully depth, welded to the web and to both flanges using fillet welds with a weld height of 8 mm. The stiffeners were set on one side of the web with an interval spacing of 130 mm, which satisfied the requirement of the AISC 341-10 provisions [15]. To prevent premature fracture at the region where the flange-to-web CJP groove weld and the fillet welds of the stiffener meet, the vertical fillet welds of the web stiffeners were terminated at a distance of five times the web thickness from the toe of the flange-to-web weld. As the length ratio of the steel beam was less than 1.0, a large overstrength factor Ω = 1.9 was assumed in prediction of its maximum shear strength capacity, as suggested by Ji et al. [5].

Table 1. Design parameters of test specimens.

Spec. no.	Design failure mode	Steel coupling beam			Beam-to-wall joint		
		Cross section (mm)	Length ratio $2a/(M_{pb}/V_{pb})$	Nominal inelastic strength (kN)	Steel web panel thickness (mm)	Horizontally distributed rebars	Beam shear load at nominal joint strength (kN)
SRC1	Joint panel shear failure	I 500×240 ×12×30	2.98	772	12	D10@150	655
SRC2	Shear yield & failure of steel	I 400×240 ×7×35	0.81	473	24	D10@150	1037

	beam						
SRC3	Joint panel shear failure	I 500×240 ×12×35	2.52	892	12	D12@100	661

2.4. Coupling beam-to-wall joints

As shown in Fig. 1(b), the flanges and web of the steel beam were connected to the column flange via complete-joint-penetration (CJP) groove welds. The horizontal stiffeners at the beam flange height were welded to the column flanges and web via CJP groove welds. The specimens SRC1 and SRC3 were designed to fail in the beam-to-wall joints. Therefore, the beam shear force corresponding to the nominal joint strength was lower than the nominal inelastic strength of steel beams for these two specimens, as listed in Table 1. The nominal joint strength was calculated based on the design model described in Section 4.

The specimen SRC2 was designed to yield and fail in the steel coupling beam. Therefore, the nominal joint strength of SRC2 was proportioned to be 15% higher than the overstrength capacity (i.e., ΩV_{pb}) of the steel beam. For ensuring the strength capacity of beam-to-wall joint, two 6 mm-thick cover plates were welded to both sides of the steel web panel of SRC2 joint using fillet welds.

Fig. 2 shows a photograph of the reinforcement details of beam-to-wall joint. The joint transverse hoops passed through the holes in the web of the embedded steel beam. The joint crossties were welded to both sides of the web panel. The horizontally distributed rebar was extended to the wall boundary with 90° hooks engaging the vertical edge reinforcement. Although the face-bearing plate is recommended by the AISC 341-10 provisions, it was not adopted in the test specimens because the addition of face-bearing plate would lead to extreme difficulty for pouring concrete. The research by Song [16] indicated that the face-bearing plate had limited effect to the strength capacity of steel coupling beam-to-SRC wall joints.

Fig. 2. Photograph of steel beam-to-SRC wall joint details.

2.5. Material properties

Per the Chinese code GB 50010-2010 [22], the concrete material properties are based on the tests of cube of 150 mm size. The measured mean value (standard deviation) of the wall concrete cubic compressive strength f_{cu} for five cubes was 75.6 (3.85), 43.7 (2.39) and 44.2 (3.02) MPa for specimens SRC1, SRC2 and SRC3, respectively. The values of f_{cu} was measured on the day of specimen testing. The axial compressive strength of concrete f_c was taken as $0.76f_{cu}$ in accordance with the GB50010-2010 code [22].

The rebar was deformed steel bars, and it complied with requirements of the International Standard of Steel for the Reinforcement of Concrete – Part 2: Hot Rolled Ribbed Bars (ISO 6935-2:2015) [23]. All rebar had a strength grade of HRB400 (nominal yield strength $f_{y,n}$ = 400 MPa). The encased steel columns were fabricated from Grade Q345 ($f_{y,n}$ = 345 MPa) steel. The steel coupling beams of specimens SRC1 and SRC3 were fabricated from Grade Q345 steel as well. The steel coupling beam of specimen SRC2 adopted the hybrid section, where the flanges were made of Q345 steel and the web of Grade Q235 ($f_{y,n}$ = 235 MPa) steel. The web stiffeners for all specimens were made of Q235 steel. The mean values and standard deviation of material properties for steel rebar and structural steel are summarized in Tables 2 and 3, respectively. The values of material properties in the tables are obtained by five standard rebar tensile tests or five tensile coupon tests of steel plates.

Table 2. Material properties for steel rebar.

Rebar	Diameter (mm)	Yield strength f_y (MPa)	Ultimate strength f_u (MPa)	f_y/f_u	Uniform elongation (%)
Wall web crossties	8	438 (18.7)	686 (9.0)	0.64	9.5 (1.5)
Horizontally distributed rebar & boundary transverse rebar	10	400 (19.3)	633 (21.1)	0.63	10.7 (2.5)
Vertically distributed rebar	12	462 (23.2)	622 (9.8)	0.74	9.8 (2.0)
Boundary longitudinal rebar	18	482 (28.0)	623 (45.3)	0.77	10.4 (0.6)

Note: The uniform elongation of rebars represents the measured strain corresponding to the peak stress of the rebar. The listed strength and elongation values are the mean values of the test results and the values in parentheses are the standard deviations.

Table 3. Material properties for structural steel.

Steel type	Plate	Thickness (mm)	Yield strength f_y (MPa)	Ultimate strength f_u (MPa)	f_y/f_u	Elongation (%)
Q235	Beam web of SRC2	7	341 (4.3)	453 (4.3)	0.75	23.2 (0.9)
	Beam stiffener	10	288 (7.3)	405 (1.4)	0.71	25.0 (1.0)
Q345	Panel cover plate for SRC2	6	408 (0.1)	555 (5.0)	0.74	20.9 (0.5)
	Beam web of SRC1 & SRC3 and web of encased columns	12	363 (21.4)	548 (33.9)	0.66	21.5 (1.7)
	Flange of encased columns	20	371 (14.72)	578 (3.84)	0.64	23.0 (2.8)
	Beam flange of SRC1	30	348 (14.3)	481 (5.0)	0.72	27.3 (2.0)
	Beam flange of SRC2 & SRC3	35	360 (5.3)	518 (0.5)	0.69	26.3 (0.9)

Note: The elongation of steel was measured after rupture along a 200-mm gauge length including the fracture zone. The listed strength and elongation values are the mean values of the test results and the values in parentheses are the standard deviations.

2.6. Test setup and instrumentation

The test specimens were loaded using the multi-functional large-scale testing facility at Tsinghua University. Fig. 3 shows the test setup. The foundation beam was securely clamped to the reaction floor. A rigid steel beam was placed between the wall's top beam and vertical actuator to distribute the vertical axial force uniformly along the wall section. The vertical axial compressive load was applied to the wall pier initially, and it was then maintained constantly for the duration of testing. Afterwards, cyclic shear loads were applied by the vertical actuators at the steel cantilever beam tip to produce force demands to the beam-to-wall joint. As shown in Fig. 3, a steel frame in the wall's perpendicular direction and the rollers attached to this frame were used to provide the constraint to the out-of-plane deflections and twisting of the steel coupling beam during testing.

In accordance with the Chinese Code for Design of Composite Structures (JGJ 138-2016) [24], the axial force ratio n of SRC walls is defined as

$$n = \frac{N}{f_c A_c + f_y A_a} \tag{1}$$

where N denotes the axial compressive load applied on the wall; f_c denotes the axial compressive strength of concrete; f_y denotes the yield strength of the encased steel column; and A_c and A_s denote the cross-sectional areas of the concrete and encased steel column, respectively. The axial compressive loads applied to specimens SRC1 and SRC3 were 2370 and 1410 kN, resulting in the axial force ratio equal to 0.05 and 0.045, respectively. The compressive load applied to specimen SRC2 was 2840 kN, corresponding to an axial force ratio of 0.09. As described in the late Subsection 5.3, numerical simulation indicates that such variation of axial compressive loads on walls have limited influence on the strength of steel beam-to-SRC wall joints.

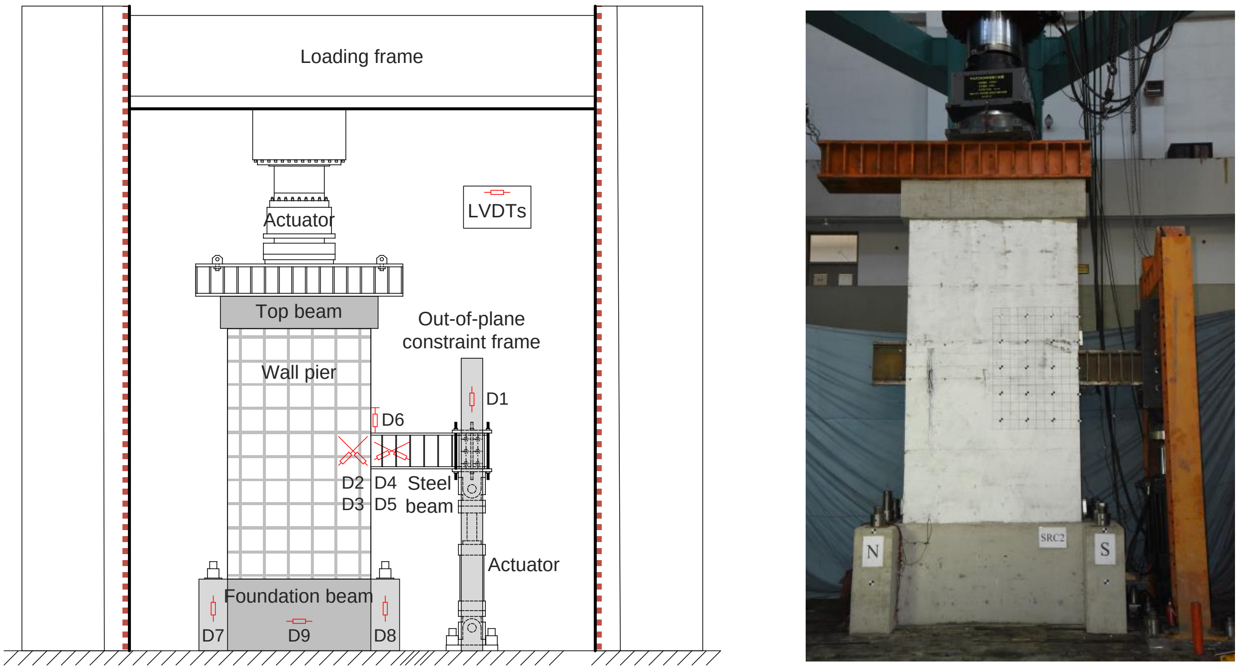

(a) Schematic drawing (b) Photograph

Fig. 3. Test setup.

Fig. 4 shows the history of shear loads applied to the steel beam, which was determined in accordance with the Chinese Specification for Seismic Test of Buildings (JGJ 101-2015) [25]. The beam shear loading was force-controlled before the specimen yielded. Four levels of loading, i.e., 0.25, 0.5, 0.75 and 1.0 times the predicted yield load $V_{y,p}$, were included in this phase. The preliminary finite element analysis predicted the yield load was approximately 480 kN for all specimens. One cycle was performed at each load level before yielding and three cycles was performed at the predicted yield load $V_{y,p}$. Afterwards, the loading was changed to be displacement-controlled. The displacement was expressed in terms of the beam rotation θ, defined as the ratio of the vertical displacement Δ at the loading point divided by the distance a from the loading point to the wall face. The displacement load was increased at increments of $\theta_{y,p,}$ where $\theta_{y,p}$ was the measured beam rotation at the predicted yield load $V_{y,p}$. Three cycles were repeated at each displacement level. In the test, push was defined as positive loading and pull as negative loading, and each push was followed by a pull for each cycle. The tests were terminated when the strength of the specimens decreased to below 85% of the peak load or the specimens sustained complete failure.

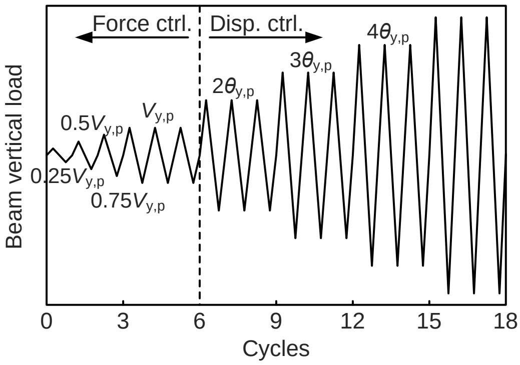

Fig. 4. Loading protocol.

Instruments were used to measure loads, displacements and strains for specimens. Load cells measured the axial compressive force applied to the wall pier and the shear force applied to the steel beam. The layout of linear variable differential transformers (LVDTs) mounted on the specimens are shown in Fig. 3(a). LVDT D1 measured the vertical displacement at the loading point of the steel beam, which was used for displacement loading control. A pair of inclined LVDTs (D2 and D3) measured the shear deformation of the joint panel. Another pair of inclined LVDTs (D4 and D5) measured the shear deformation of the steel beam. LVDT D6 was used to measure the local opening and closing of the gap at the interface between steel coupling beam flange and wall concrete. Three LVDTs (D7 through D9) were used to monitor possible rotation and horizontal slip of the foundation beam. Strain gauges were mounted in the rebar and structural steel to measure the strains of the horizontally distributed rebar, boundary longitudinal and transverse rebar in the joint region, steel web panel, and flanges and web of the steel coupling beam.

3. Experimental results

3.1. Hysteretic response

Fig. 5 shows the hysteretic and envelope curves of the beam shear force *V* versus beam rotation θ for all specimens. The yield points of reinforcement and structural steel measured by strain gauges are indicated in Fig. 5. The measured rotation and horizontal slip of the foundation beam were very small (the maximum rotations and slippage were 0.02% and 0.81 mm), which had negligible influence on the beam-to-wall joint responses. As the wall piers were much stiffer than steel beams, the global flexural deformation of wall piers was very small and had negligible influence to the beam tip displacement, which was also confirmed by the FE analysis results. Therefore, the defined beam rotation θ in Fig. 5 was contributed by the flexural and shear deformation of coupling beam, and the shear angle and rotation of the beam-to-wall joint. Unfortunately, the shear deformation of the joint panel was not measured at the large beam rotation loading, because the LVDTs 2 and 3 fell off after the concrete of joint panel sustained damage. However, the test observations implied the dominated components of the defined beam rotation θ. For specimens SRC1 and SRC3, the steel web panel, joint transverse rebar and horizontally distributed rebar yielded significantly during the loading, and thus their hysteretic curves were dominated by inelastic response of the beam-to-wall joints. For specimen SRC2, the steel beam web yielded and eventually fractured, while the web panel and joint transverse reinforcement remained nearly elastic. Therefore, its hysteretic curve was dominated by inelastic response of the steel beam.

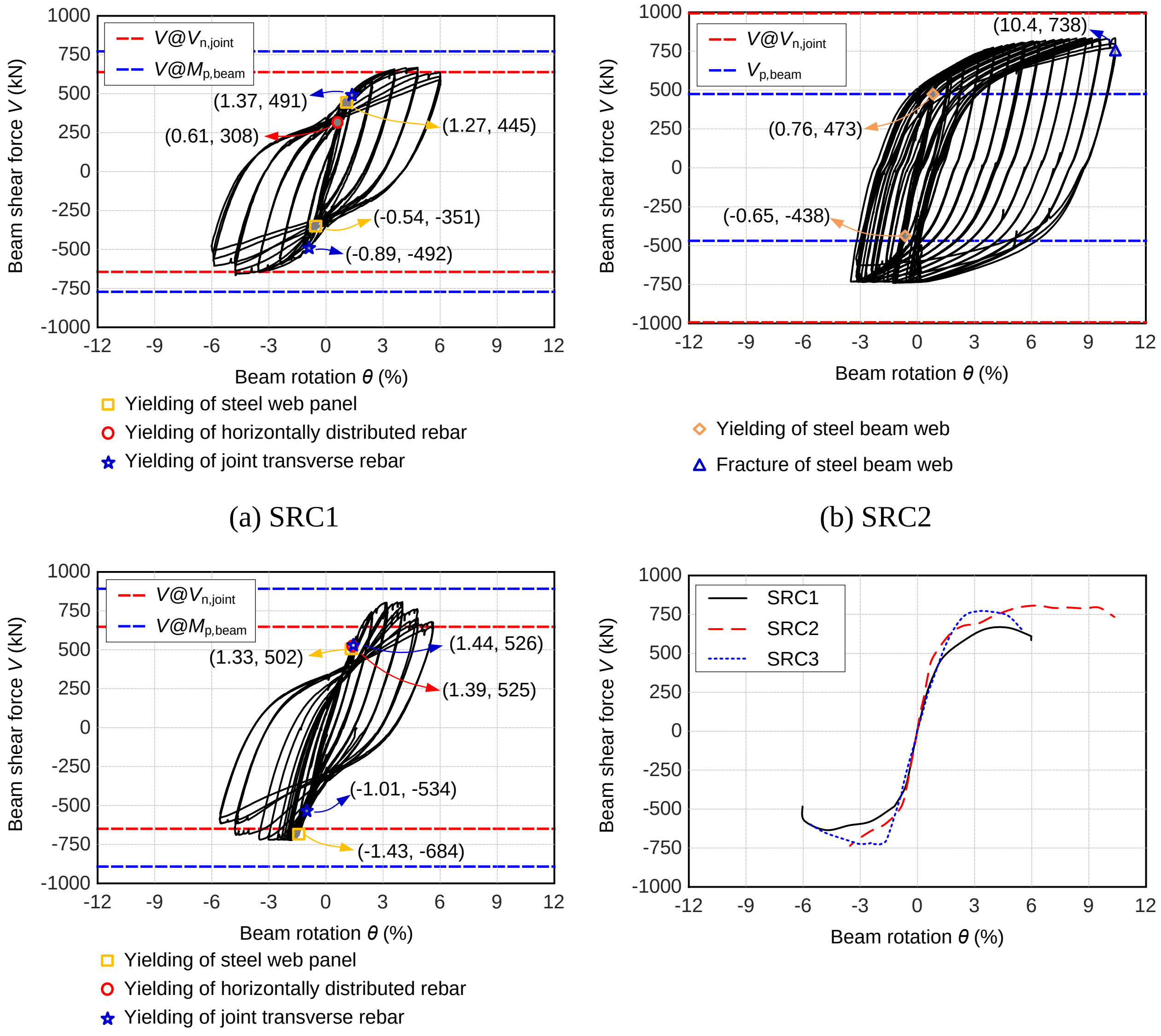

(a) SRC1 (b) SRC2

(c) SRC3 (d) Envelope curves of tested specimens

Fig. 5. Beam shear force versus beam rotation of test specimens.

Specimens SRC1 and SRC3 exhibited similar hysteretic responses. After yielding of the steel web panel and joint transverse reinforcement, the loading stiffness decreased obviously, while the strength continued to increase due to further development of the compressive strut strength of concrete panel and cyclic hardening effect of web panel steel. Before 4% beam rotation, the hysteresis curves of three loading cycles at the same displacement magnitude were nearly identical. Afterwards, the strength degradation of consecutive cycles at the same displacement loading became obvious. Specimens SRC1 and SRC3 reached their peak load at 5% and 4% beam rotation, respectively. The calculated values of beam shear forces corresponding to the nominal strength of joints ($V@V_{n,joint}$) and the nominal inelastic strength of steel beams ($V@M_{p,beam}$) are also indicated in Fig. 5. The measured maximum strength of both specimens exceeded the nominal strength of beam-to-wall joints, while it did not reach the nominal inelastic strength of steel beams. Because the actuator had the load capacity limit of 745 kN in pull, the beam shear force of specimen SRC3 in the negative loading was governed by the actuator load capacity and the joint strength did not fully developed in that loading direction. Upon to further loading, both specimens showed strength deterioration. The strain data indicated the beams behaved nearly in elastic in the duration of loading, except for slight yielding of beam flanges near the wall face.

As shown in Fig. 5(b), the hysteresis loop of SRC2 was very full and stable even under 10% beam rotation loading, which reflected the characteristics of cyclic response of steel shear link beams. The steel beam yielded in shear, and developed remarkable overstrength until the beam web fracture. The beam-to-wall joint only sustained slight damage and contributed to limited deformation. Note that, similarly as specimen SRC3, the beam shear force in the negative loading for SRC2 was governed by the pull load capacity of the actuator. After reaching this load capacity, the negative loading was changed to be force-controlled, while the positive loading remained to be displacement-controlled and followed the loading history as shown in Fig. 4.

3.2. Damage and failure mode

3.2.1. Joint failure for specimens SRC1 and SRC3

Specimens SRC1 and SRC3 sustained panel shear failure at the beam-to-wall joint, while no damage was observed in the steel beam till the joint failure. For specimen SRC1, few slight inclined cracks were observed in the joint concrete panel at the beam shear load V = 240 kN (i.e., $V_{y,p}/2$). Besides, slight cracks occurred along the inner side of wall boundary element around the joint region. Upon to the beam shear load V = 480 kN (i.e., $V_{y,p}$), crisscrossed diagonal cracks obviously developed in the concrete panel. The stain gauge data indicated the steel web panel and joint transverse reinforcement yielded prior to 1.5% beam rotation. The vertical cracks extended along the inner side of boundary element. At beam rotation θ = 3.6% loading, the concrete cover of the joint panel started to spall off and the transverse rebar was exposed. The vertical cracks along the wall boundary element extended to the entire wall height. Up to beam rotation θ = 4.8% loading, crisscross diagonal cracks subdivided the concrete panel into a series of concrete blocks separated by inclined cracks. The cyclic reversal led to spalling of concrete blocks. At beam rotation θ = 6.0%, the concrete of joint panel sustained crushing. The wide thorough cracks along the inner side of wall boundary element led to tensile fracture of the horizontally distributed rebar that crossed the cracks. Concrete cover at wall face spalled off due to bearing of the steel flanges against the concrete. Fig. 6(a) shows the photographs of beam-to-wall joints of the specimen at the end of testing.

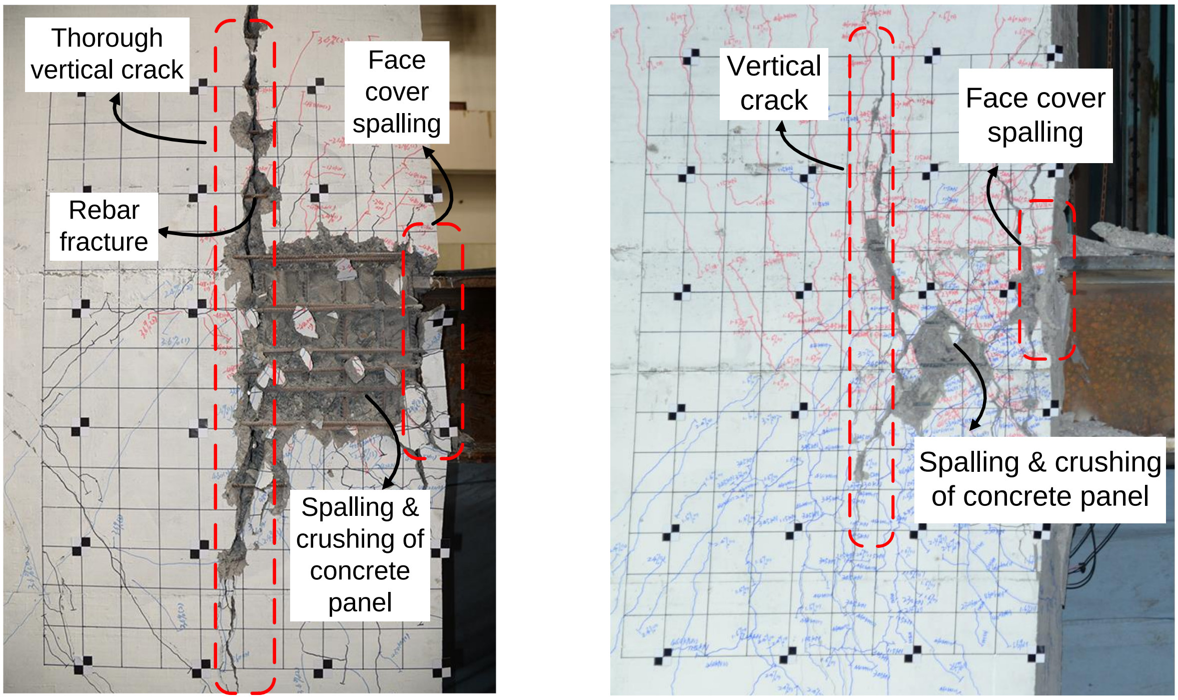

(a) SRC1 (b) SRC3

Fig. 6. Photographs of beam-to-wall joints of SRC1 and SRC3 at the end of testing.

The damage of specimen SRC3 was similar as SRC1. The specimen SRC3 failed at 5.6% beam rotation loading, due to spalling and crushing of joint panel concrete, as shown in Fig. 6(b). However, because the horizontally distributed rebar was strengthened in both above and below the joint for 1000 mm, the vertical cracks along the wall boundary element did not extend beyond this region. No reinforcement fractured during the testing of specimen SRC3.

3.2.2. Steel beam failure for specimen SRC2

At the beam shear load V = 240 kN (i.e., $V_{y,p}/2$), a few minor vertical cracks were observed at the joint panel of specimen SRC2. At V = 480 kN (i.e., $V_{y,p}$), the steel beam web yielded in shear, as indicated from strain measurement data. Diagonal cracks occurred in the joint concrete panel. The maximum crack width was less than 0.2 mm. Only cosmetic repair is required for such slight damage per the provisions of the Chinese Code for Design of Strengthening Concrete Structure (GB 50367-2010) [26].

Up to beam rotation θ = 2.4% loading, the cracks in the joint region extended and widened. Afterwards, the cracks remained stable without further development. At beam rotation θ = 7.2%, local buckling was observed in the steel beam web. At beam rotation θ = 10.4%, the fracture initiated at the termination of a fillet weld connecting a stiffener to the web. Then the fracture rapidly propagated along the stiffener-to-web weld and the web-to-flange weld, and finally tore the web apart, as shown in Fig. 7(b). The web facture failure is similar to the observations in past tests on steel link beams (e.g., Okazaki et al. [27] and Ji et al. [5]). As shown in Fig. 7(a), no severe damage (e.g., spalling of concrete and exposure of reinforcement) was observed in the beam-to-wall joint until the end of the testing. The concrete cracks had the width less than 1.6 mm. In accordance with FEMA P-58 [28], such damage of concrete cracking belongs to damage state DS1 and it can be repaired by epoxy injection of cracks. It indicates that if the steel beam-to-SRC wall joint is properly proportioned and detailed, the damage to the joint can be slight and repairable till the steel coupling beam fully develops its plastic rotation.

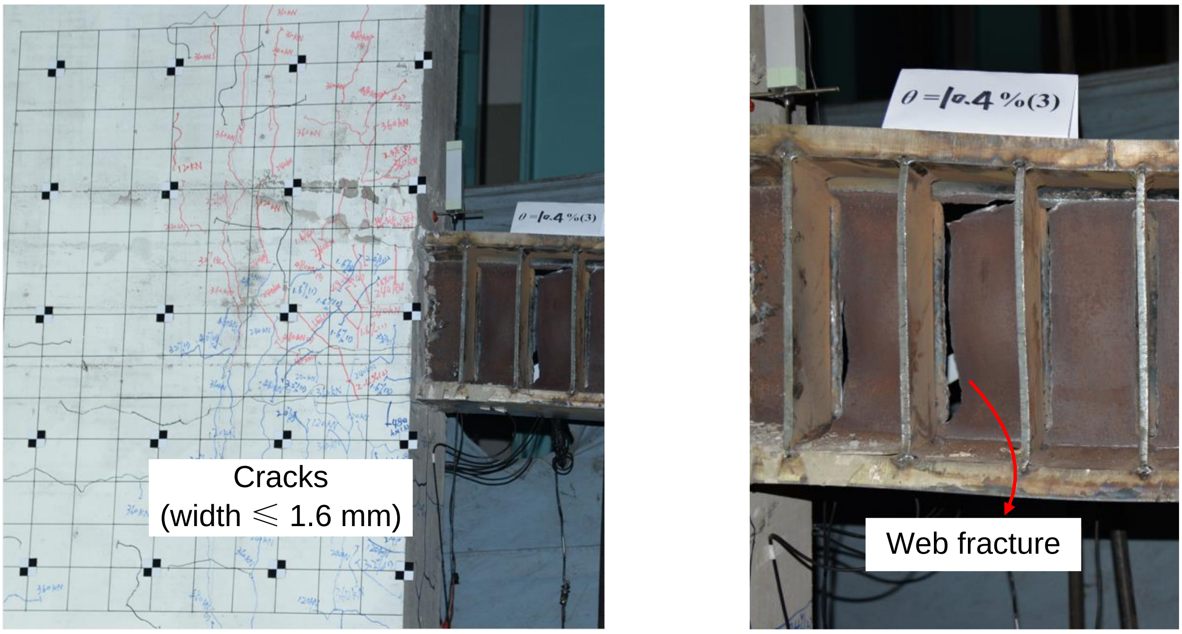

(a) Beam-to-wall joint (b) Web fracture of steel beam

Fig. 7. Photographs of SRC2 at the end of testing.

3.3. Strength and deformation capacity

Table 4 summarizes the strength and deformation capacity of all specimens. For specimens SRC1 and SRC3 that failed in beam-to-wall joints, the yield point is determined using the idealized bi-linearization of the load-displacement envelope curves as specified in ASCE/SEI 41-13 [29]. For specimen SRC that failed in steel coupling beam, the defined yield point corresponds to the plastic shear strength of steel coupling beam as specified in AISC 341-10 [15]. For specimen SRC3, its ultimate deformation (i.e., the ultimate beam rotation θ_u) is defined as the post-peak displacement at the instant when the beam shear load decreases to 85% of the peak load [25]. As the post-peak strength of specimens SRC1 and SRC2 did not decrease below 85% of the peak load till failure, the ultimate beam rotation is defined as the maximum displacement that the specimen endured within a full cycle before failure. Note that, the values of the peak load (V_{max}) and corresponding beam rotation (θ @ V_{max}), and ultimate beam rotation (θ_u) for specimens SRC2 and SRC3 were obtained from the positive loading, because the negative loading was governed by the actuator pull load capacity. Other results listed in Table 4 are the average values measured from both positive and negative loading.

The following observations are obtained from Table 4. (1) The maximum shear strength capacity V_{max} of steel beam in SRC2 was 1.76 times its plastic shear strength V_{pb}. This large overstrength is in good agreement of past test data on very short shear links [5]. (2) The yield and maximum strengths of specimen SRC3 were larger than the values of SRC1, due to the contribution of increased amount of horizontally distributed rebar at the joint region. (3) Specimen SRC1 had larger values of θ_p and θ_u, compared with SRC3. This is because the vertical cracks that significantly developed along the wall boundary element in SRC1 resulted in additional joint rotation angle.

Table 4. Test result of the strength and deformation capacity

Spec. no.	V_y (kN)	θ_y (%)	V_{max} (kN)	θ @ V_{max} (%)	θ_u (%)
SRC1	525	1.04	669	4.79	5.95
SRC2	450	0.69	834	10.4	10.4
SRC3	674	1.59	807	3.99	5.49

The deformation capacity of steel beam-to-SRC wall joints obtained in this study is compared with the measured results in past tests. Specimens SRC1 and SRC3 had larger ultimate rotation capacity θ_u than the specimen CF-1 in Song [16] and specimen CW in Li et al. [18] of which the ultimate beam rotation was approximately 3%. Although specimens CF-1 and CW used the fully weld connection details as well, specimen CF-1 failed due to premature fracture of horizontal stiffener to column flange welds and specimen CW failed due to tensile fracture of horizontally distributed rebar of wall pier. This highlights the significance of weld details and horizontally distributed rebar around joints.

In the tests by Wu et al. [17], another type of steel beam-to-SRC wall joints was adopted, where the steel beams were connected to the encased steel columns using an end-plate connection with high-strength bolts. Both steel coupling beams and beam-to-wall joints yielded significantly in those test specimens, and the contribution of beam-to-wall joints on the beam rotation was not measured. Therefore, direct comparison of deformation capacity for the two types of joints is not available. Nevertheless, all specimens in [17] failed due to the fracture of end plates, which resulted in a sudden drop of joint strength capacity. Additional calculation using the model presented in Section 4 indicates that all specimens did not fully developed their panel shear strength capacity of the joints due to premature fracture of the end plates. Therefore, further development of design method and details of the beam-to-wall joints using an end-plate connection is needed.

4. Design model of steel beam-to-SRC wall joint strength

4.1. Design model of joint strength

The panel shear failure mechanism of the steel coupling beam-to-SRC wall joint is similar as that of the reinforced concrete column-to-steel beam (RCS) joint. Analogous to the model proposed by Deierlein et al. [30] for estimating the panel shear strength of RCS joints, Li et al. [19] proposed the model for calculating the nominal strength of steel coupling beam-to-SRC wall joints. Fig. 8 shows the schematic view of the panel shear failure mechanism of the steel beam-to-SRC wall joint.

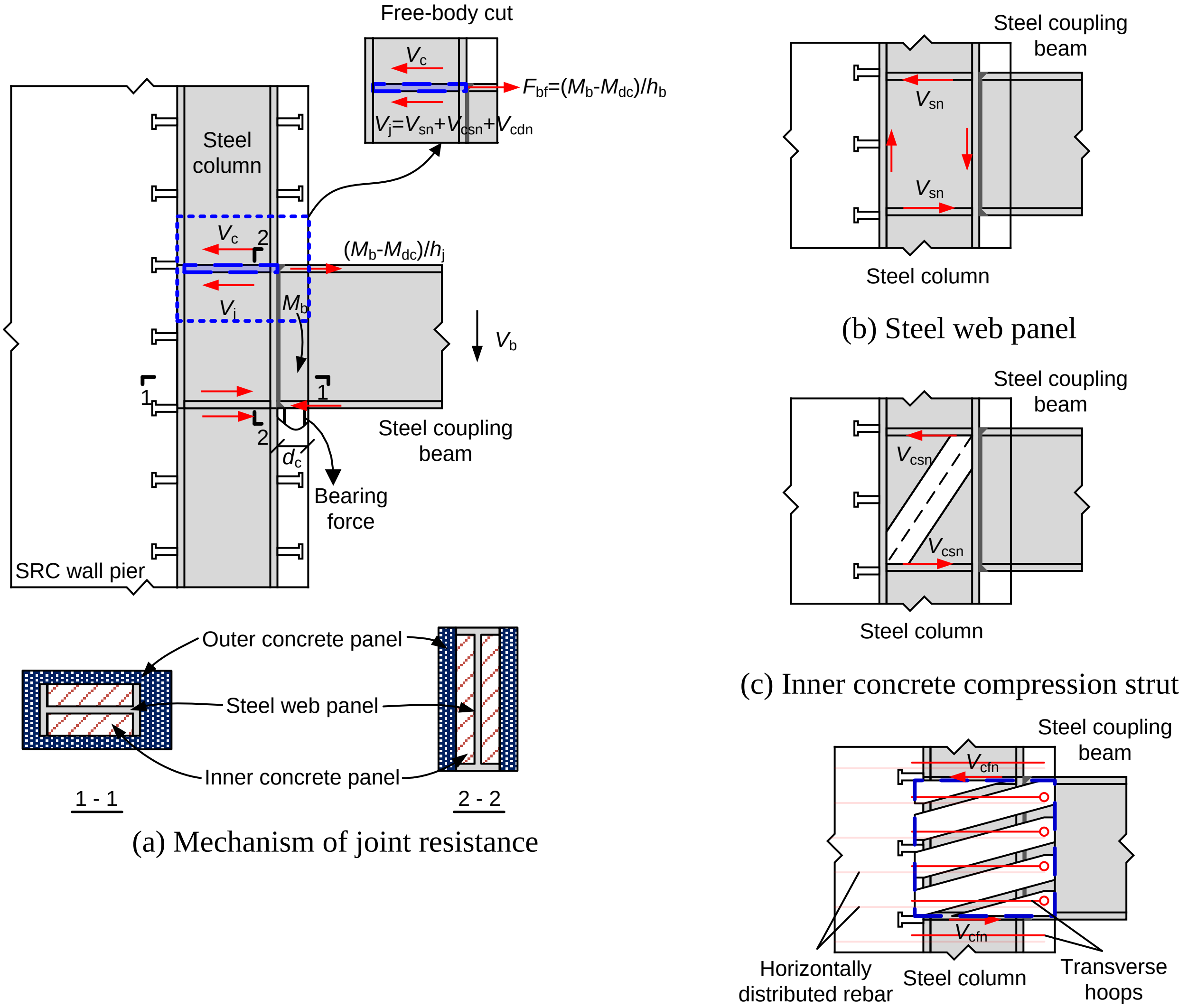

(a) Mechanism of joint resistance

(b) Steel web panel

(c) Inner concrete compression strut

(d) Outer concrete compression field

Fig. 8. Panel shear mechanism of steel beam-to-SRC wall joint

As shown in Fig. 8(a), beam moment is shown as equivalent horizontal force couples acting in the beam flanges. The joint shear mechanisms are visualized by considering their role in resisting the horizontal beam flange forces and thus preventing horizontal movement of the beam flange. Based on the free-body cut shown in the blue dashes in Fig. 8(a), Eq. (5) is obtained from the horizontal force equilibrium.

$$V_c + V_j = F_{bf} \tag{2}$$

where V_c denotes the shear resistance provided by the upper column, V_j denotes the shear resistance of the joint panel, and F_{bf} denotes the horizontal tensile force of beam flange. Below describes the calculation of these three items.

(1) Horizontal force of beam flange (F_{bf})

The horizontal force acting in the beam flange, F_{bf}, is related to beam moment demand, given by:

$$F_{bf} = (M_b - M_{dc}) / h_b \tag{3}$$

where $M_b = V_b l_b$ denotes the bending moment demand of the beam at column flange, V_b denotes the beam shear load, l_b denotes the distance of the vertical loading point to the column flange, M_{dc} denotes the moment resistance provided by bearing action of compressive concrete within the embedment distance of steel beam (see Fig. 8(a)), and h_b denotes the sectional depth of steel beam.

Using the equivalent rectangular compressive stress block of bearing concrete, M_c can be calculated as follows [19]:

$$M_c = \beta_1 d_c f_b b_f \cdot (1 - \beta_1 / 2) d_c \tag{4}$$

where d_c denotes the embedment distance of steel beam (see Fig. 8(a)); b_f denotes the width of the steel beam flange; β_1 denotes the equivalent stress block parameter and its value can be determined per the ACI 318-14 provision; and f_b denotes the bearing strength of concrete, given by [13]:

$$f_b = 4.5\sqrt{f_c}\left(\frac{t_{wall}}{b_f}\right)^{0.66} \tag{5}$$

where f_c denotes the axial compressive strength of the concrete (unit in MPa), and t_{wall} denotes the wall thickness.

(2) Shear resistance provided by column (V_c)

The column shear is governed by the minimum value of the shear yield strength of steel column web (V_{pc}) and the resultant tensile strength of horizontally distributed rebar in the wall's horizontally tensile region (V_{hr}) that provides the horizontal restraint to the boundary element [19]. Therefore, the nominal strength of column V_c is calculated as follows:

$$V_c = \min\left(V_{pc}, V_{hr}\right) \tag{6-a}$$

$$V_{pc} = 0.6 f_{cw} h_{cw} t_{cw} \tag{6-b}$$

$$V_{hr} = \sum f_{yhr} A_{hr} \tag{6-c}$$

where f_{cw} denotes the yield strength of column web steel, h_{cw} denotes the height of column web, t_{cw} denotes the thickness of column web, and f_{yhr} and A_{hr} denotes the yield strength and cross-sectional area of horizontally distributed rebar in the wall's horizontally tensile region.

The value of V_{hr} was slightly higher than V_{pc} for specimen SRC1, while the former was approximately twice higher than the latter for specimen SRC3.

(3) Shear resistance of joint panel (V_j)

Similar to the reinforced concrete column-to-steel beam joint by Deierlein et al. [30], the panel shear strength V_j is contributed by three components: (a) steel web panel resistance V_{sn} (see Fig. 8(b)); (b) concrete compression strut mechanism V_{csn} developed in the inner concrete panel (see Fig. 8(c)); and (c) concrete compression field mechanism V_{cfn} developed in the outer concrete panel (see Fig. 8(d)). Therefore, the nominal strength of V_j can be calculated as follows:

$$V_j = V_{sn} + V_{csn} + V_{cfn} \tag{7}$$

(a) Shear resistance of steel web panel V**sn:** The nominal strength of steel web panel V_{sn} is calculated as follows:

$$V_{sn} = 0.6 f_{yp} h_p t_p \tag{8}$$

where f_{yp} denotes the yield strength of the steel web panel, h_p denotes the clear depth of the web panel, and t_p denotes the steel web panel thickness.

(b) Shear resistance of inner concrete compression strut V**csn:** The concrete compression strut mechanism is mobilized by the horizontal stiffeners and column flanges, which bear against the concrete when the joint and steel panel deform in shear (see Fig. 8(c)). According to the ASCE guideline for design of joints between steel beams and RC columns [31], the nominal strength of the concrete compression strut mechanism V_n is calculated by

$$V_{csn} = 1.7\sqrt{f_c}b_i h_c \le 0.5 f_c b_i h_{bw} \quad (9)$$

where f_c denotes the axial compressive strength of concrete (unit in MPa), $b_i = b_{cf} - t_p$ denotes the width of inner concrete panel, b_{cf} denotes the flange width of steel column, h_c denotes the section height of the embedded steel column, and h_{bw} denotes the web height of steel beam.

***(c) Shear resistance of outer concrete compressive field V_{cfn}*:** The concrete compressive field is mobilized in outer concrete panel (i.e., the boundary element region outside the column flanges and horizontal stiffeners, as shown in Fig. 8(a)). The mechanism is similar to truss model for shear in RC members (see Fig. 8(d)). As the wall thickness is not significantly larger than the embedded steel column flange width, nearly all concrete in the outer panel can be effective as compression struts of the truss mechanism, which is also verified by the FE analysis. The shear strength is calculated by the sum of the concrete and joint transverse reinforcement. Per the ASCE guideline for design of joints between steel beams and RC columns [31], the horizontal shear strength V_{cfn} is calculated by

$$V_{cfn} = 0.9 f_{ysh} A_{sh} h_j / s_{sh} + 0.4\sqrt{f_c} A_{outer} \le 1.7\sqrt{f_c} A_{outer} \quad (10)$$

where f_{ysh}, A_{sh} and s_{sh} denote the yield strength, cross-sectional area and spacing of joint transverse reinforcement (including boundary transverse rebar and horizontally distributed rebar in the joint panel), respectively; f_c denotes the axial compressive strength of concrete (unit in MPa); h_j denotes the depth of joint, which is taken as the extent of wall boundary element; A_{outer} denotes the cross-sectional area of outer concrete panel.

Substituting Eqs. (3) through (10) into Eq. (2), the nominal strength capacity of the steel beam-to-SRC wall joint and the corresponding beam shear force V_b can be estimated.

4.2. Validation with test data

The design model for calculating the nominal strength of steel beam-to-SRC wall joints is validated with the test data. Fig. 9 shows the calculated nominal strengths for specimens SRC1 and SRC3, compared with the experimental results. The strength contribution of each component is also plotted in this figure. The design model provides a reasonable estimate of the joint strength capacity. The calculated beam shear force V_{cal} at joint nominal strength is equal to 98% and 82% of the test value for specimens SRC1 and SRC3, respectively. Table 5 further compares the calculated strength with the experimental data collected from past tests and this experimental program. The design model provides reasonable and conservative estimation of the strength of steel beam-to-SRC wall joints. The mean value of the ratio of experimental-to-calculated strength V_{test}/V_{cal} is 1.11, and the standard deviation of the ratio V_{test}/V_{cal} is 0.15. Note that the ratio of V_{test}/V_{cal} for specimen CF-1 in Song [16] is less than 1.0. It is likely because the premature weld fracture of this specimen impeded the full development of the joint panel shear strength capacity.

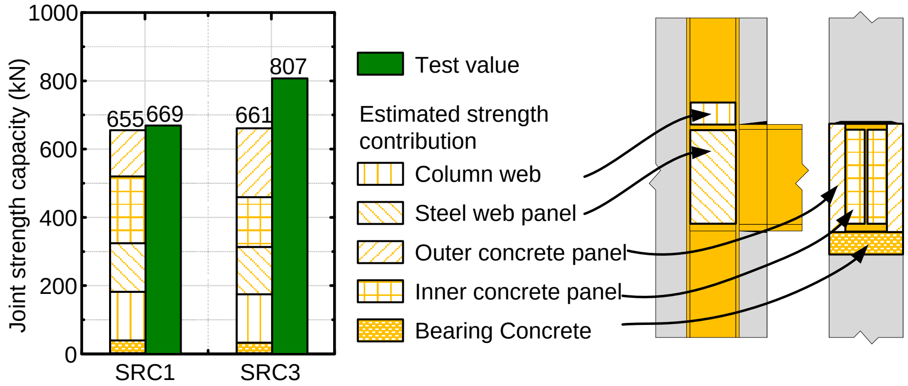

Fig. 9. Estimated strength capacity for specimens.

Table 5. Comparison of experimental versus calculated strengths for specimens

Ref.	Spec. no.	Shear strength (kN)		V_{test}/V_{cal}
		Calculated V_{cal}	Experimental V_{test}	
Song [16]	CF-1	471	423	0.90
Li et al. [18]	CJ	618	766	1.24
	CW	618	727	1.17

This paper	SRC1	655	669	1.02
	SRC3	661	807	1.22
			Mean	1.11
			Standard deviation	0.15

5. Finite element analysis

5.1. Finite element model

Finite element (FE) analysis was performed to further validate the mechanism and accuracy of the design model for joint strength. The FE models of specimens SRC1 and SRC3 were developed using the ABAQUS 6.10 program [32]. The concrete wall, steel beam and encased steel column were discretized using 8-node reduced integration (C3D8R) solid elements, and the rebar was represented by 3-dimensional 2-node truss (T3D2) elements. The meshing of the finite element model is shown in Fig. 10. Mesh sensitivity studies showed the convergence of the model.

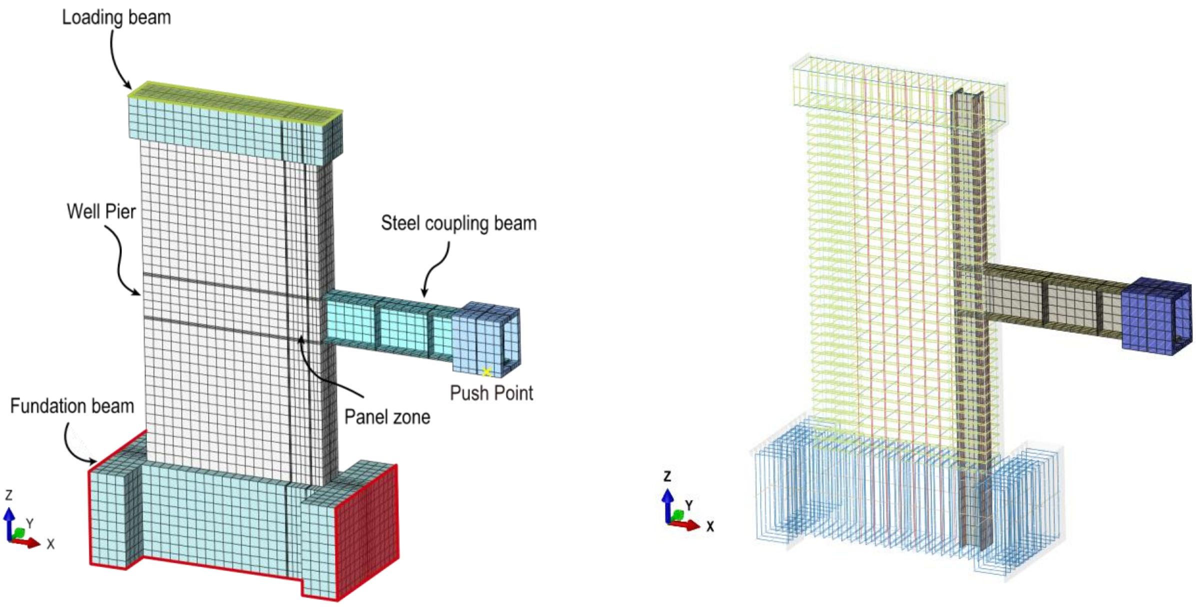

(a) Whole model (b) Rebar and structural steel

Fig. 10. Finite element model of specimen.

The concrete material was simulated by the concrete damaged plasticity model. The uniaxial compressive and tensile stress-strain relationships of concrete were determined per the Chinese code GB 50010-2010 [22]. The axial compressive strength f_c and the axial tensile strength f_t of concrete was taken as $f_c = 0.76f_{cu}$ and $f_t = 0.395f_{cu}^{0.55}$ respectively, in accordance with GB 50010-2010, where f_{cu} adopted the mean value of measured cubic strength of concrete. Table 6 summarizes the values of other parameters of the concrete damaged plasticity model defined in the numerical models.

Table 6. Parameters of the concrete damaged plasticity model.

Model parameters	Values
Poisson's ratio	0.2
Dilation angle	30°
Eccentricity	0.1
f_{b0}/f_{c0}, the ratio of initial equibiaxial compressive yield stress to initial uniaxial compressive yield stress	1.16
K_c, the ratio of the second stress invariant on the tensile meridian to the compressive meridian	2/3
Viscosity parameter	0.005

The stress-strain relation of rebar was simulated by a bilinear model for simplicity, where the Young's modulus was taken as 2.0×10^5 MPa, and the post-yield modulus as 2.45×10^3 MPa. The yield strength of each type of rebar was taken as the mean value of the measured yield strength by standard rebar tensile tests (see Table 2). The steel plate was simulated by the plasticity model, where the von-Mises criteria is used to determine the yield surface of steel. The Young's modulus and Poisson's ratio of the steel were taken as 2.1×10^5 MPa and 0.3, respectively. The strength of steel was taken as the mean value of measured strength by steel tensile coupon tests (see Table 3). The uniaxial stress-strain relation of structural steel was simulated using the Ramberg-Osgood model as shown in Eq. (11), which reflects cyclic hardening effect of steel.

$$\varepsilon_s = \frac{\sigma_s}{E_s} + \left(\frac{\sigma_s}{K}\right)^{1/n} \tag{11}$$

where σ_s and ε_s denotes the uniaxial stress and strain of steel plate, E_s denotes the Young's modulus of steel, and K and n are the parameters, taken as 1020 and 0.138 respectively for Q345 steel as suggested by Dusicka et al. [33].

The interaction between structural steel and concrete was simulated using surface-to-surface contact, where "hard" contact was assigned in the normal direction and Coulomb friction with a penalty friction coefficient of 0.6 was assigned in the tangential direction. Steel rebar was connected to the concrete using "embedded" constraint, without consideration of bond slippage.

The foundation beam was fixed at its bottom and edge faces. Similarly as the test program, the axial compressive load was initially applied to the top beam of the wall pier by uniformly distributed loads. Afterwards, the cantilever steel beam was loaded at the beam tip using displacement-load control. Allowing for the computational efficiency, the monotonic loading was adopted instead of the cyclic loading. Both material and geometric nonlinearity were accounted for in the analysis. Newton-Raphson method was adopted to solve the nonlinearity problem.

5.2. Analytical results

Fig. 11 shows the analytical monotonic curves of the beam shear force versus beam rotation, compared with the experimental hysteretic curves. The calculated yield points of steel reinforcement and plates are also shown in the figure. The FE analysis results correlated well with the test data. Because the monotonic loading in the FE analysis did not reflect the cumulative damage effect of concrete induced by cyclic loading, the strength degradation was not observed in the analytical results. Therefore, the strength capacity of the FE model is defined as the strength at 4.0% beam rotation, which is close to the experimental beam rotation at peak load. The difference between the analytical and experimental values of the strength capacity was less than 10%.

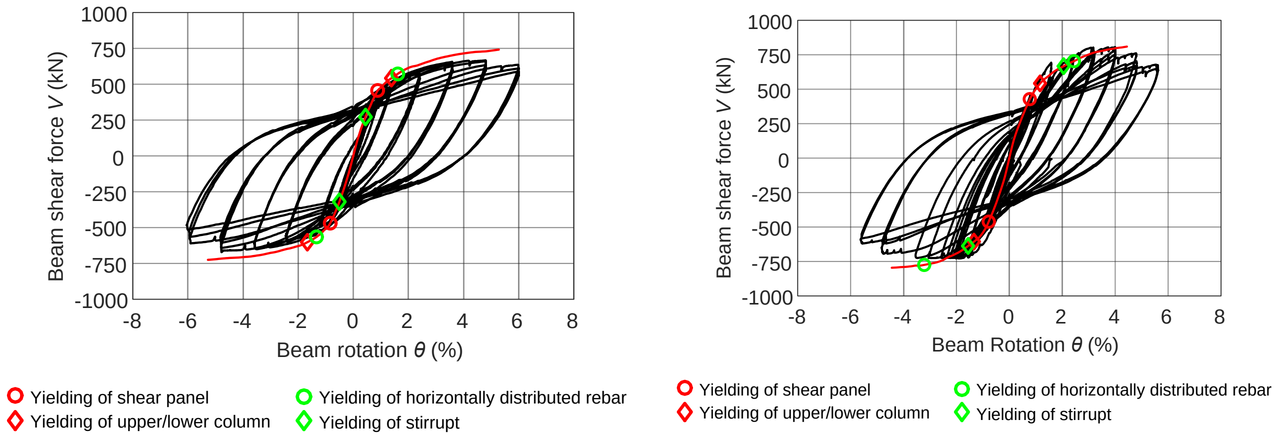

(a) SRC1 (b) SRC3

Fig. 11. Analytical curves of shear load versus beam rotation for specimens.

Fig. 12 shows the deformation, strain and stress of the SRC1 model at 4% beam rotation in the positive loading. As shown in Fig. 12(a), severe plasticity occurred in the joint panel concrete. The bearing concrete beneath the lower flange of embedded steel beam also developed plasticity. Fig. 12(b) indicates the points at the instant when the steel web panel and upper column web yielded in shear. Joint transverse rebar and horizontally distributed rebar obviously yielded, which forms the ties of the truss mechanism. The outer panel concrete developed high diagonal compressive stress (see Fig. 12(d)), to serve as the compressive struts of the truss mechanism. A section-cut of the inner concrete panel (see Fig. 12(c)) indicates high principal compressive stress of the concrete developed in the diagonal direction to form the inner compressive strut mechanism. The FE analytical results validates the mechanisms assumed in the design model of joint strength.

Fig. 13 shows the deformation, strain and stress of the SRC3 model. Comparison between Figs. 12 and 13 indicates the extent of concrete plasticity (representing the vertical cracks) along the inner side of boundary element of SRC3 model was shorter than SRC1 model. It is consistent with the test observations. The increased horizontally distributed rebar around the joint showed benefit of controlling the vertical cracks.

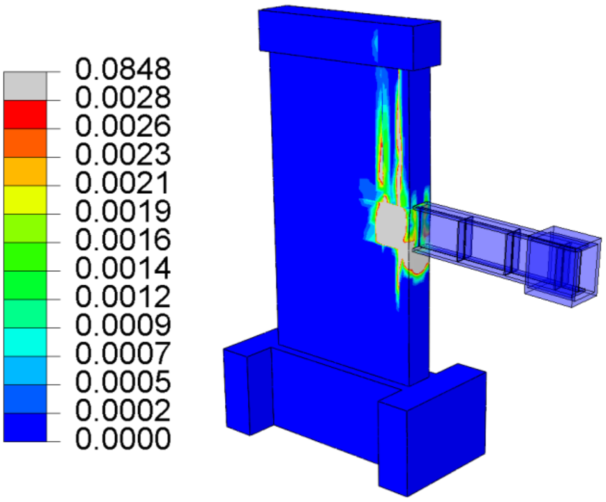

(a) Equivalent plastic strain of concrete

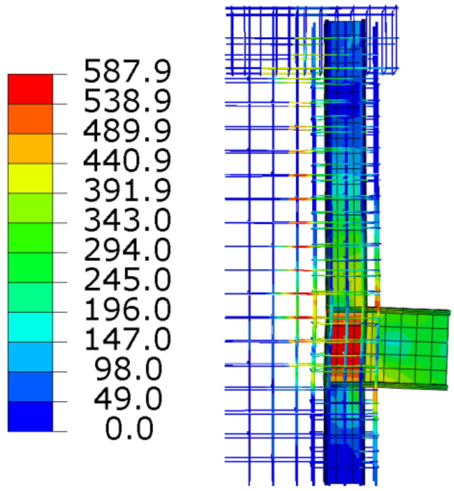

(b) Equivalent plastic strain of reinforcement and structural steel

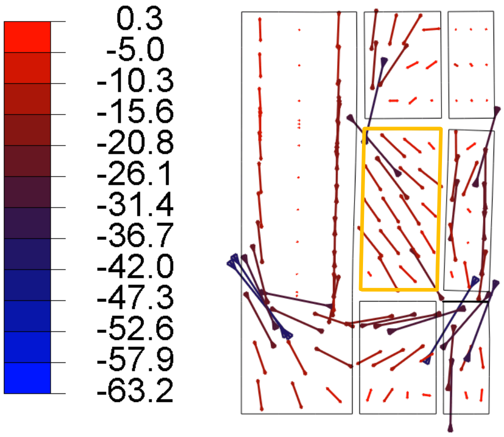

(c) Principal compressive stress of inner concrete

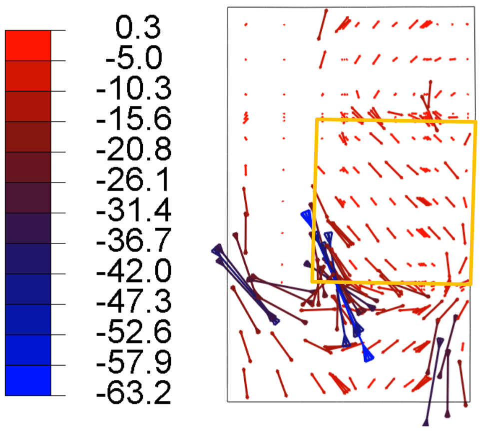

(d) Principal compressive stress of outer concrete

Fig. 12. Strain and stress distribution of SRC1 model at 4% beam rotation load.

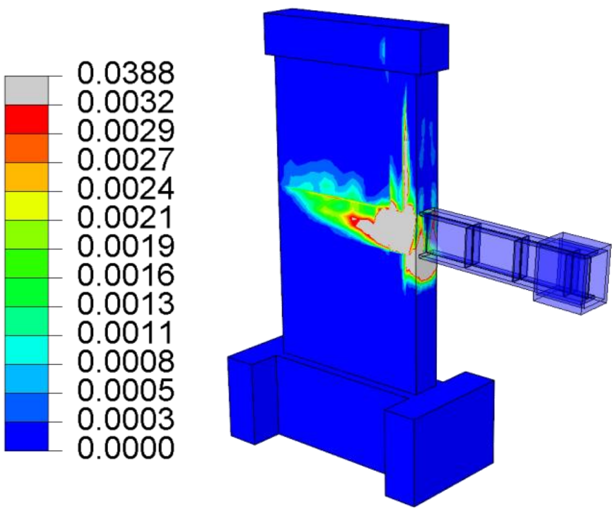

(a) Equivalent plastic strain of concrete

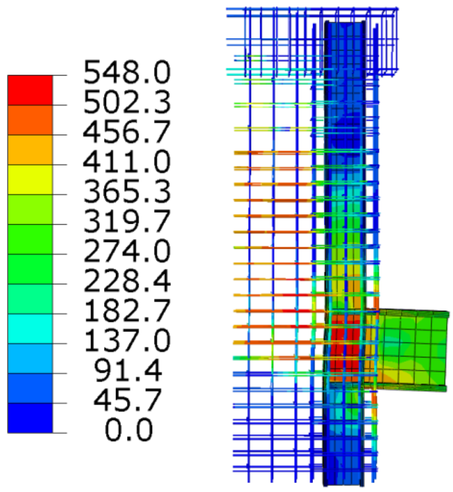

(b) Equivalent plastic strain of reinforcement and structural steel

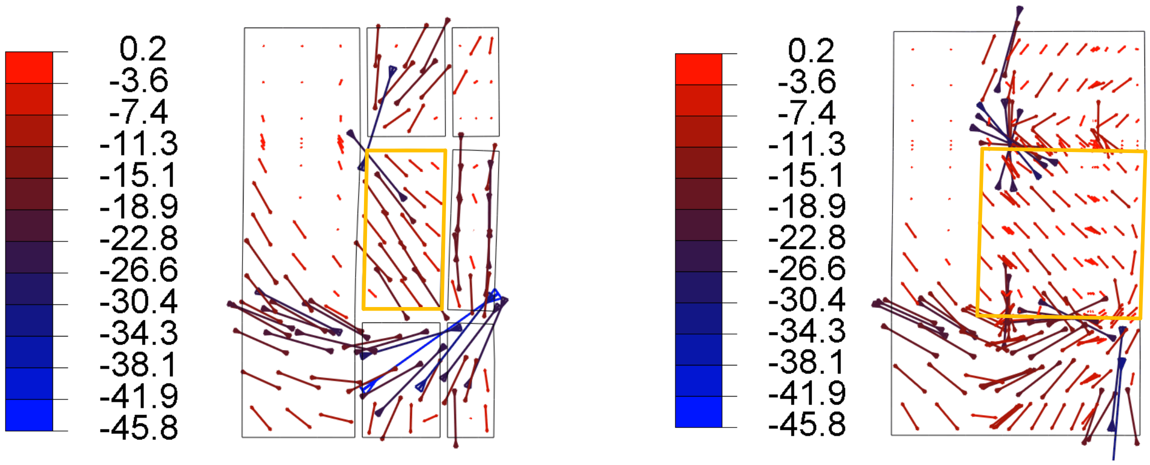

(c) Principal compressive stress of inner concrete (d) Principal compressive stress of outer concrete

Fig. 13. Strain and stress distribution of SRC3 model at 4% beam rotation load.

5.3. Parametric analysis of joint strength

Additional parametric analysis was implemented to obtain more data for further calibration of the design model of joint strength. The FE model had identical geometric dimensions as specimens SRC1 and SRC3. The following design parameters were considered as variables in the analysis: (a) concrete strength (the axial compressive strength f_c ranging from 23 to 48 MPa); (b) steel web panel thickness (ranging from 8 to 16 mm); (c) reinforcement ratio of horizontally distributed rebar (ranging from 0.31% to 0.65%); (d) axial force ratio (ranging from 0 to 0.3). A total of 30 models were included in the parametric analysis. All models failed in panel shear mode of beam-to-wall joints.

Fig. 14 plots the nominal strength calculated by the design model (V_{cal}), compared with the collected test data and FE analytical results ($V_{T,FEA}$). All experimental and FE analytic values of joint strength were larger than the calculated value of the design model, except for the test specimen CF-1 in Song [16] that failed in premature weld fracture. The ratio of $V_{T,FEA}/V_{cal}$ had the mean of 1.16, and the standard deviation of 0.08. Therefore, the design model provides a reasonable and conservative estimate of the strength of steel beam-to-SRC wall joints.

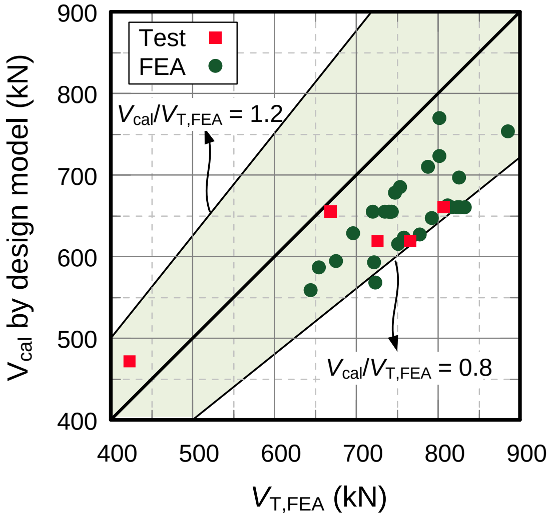

Fig. 14. Comparison between calculated nominal strength and experimental or FE results

6. Conclusions

This paper has presented a series of quasi-static tests on full-scale steel coupling beam-to-SRC wall subassemblies. The cyclic behavior and strength capacity of steel beam-to-SRC wall joints were investigated. The design model for calculating the nominal strength of the joints was presented and the accuracy of the model was validated by comparison with collected test data and finite element (FE) analysis using ABAQUS program. The major findings of this study are summarized as follows:

(1) The steel coupling beam-to-SRC wall joint failed in panel shear mode, characterized by crisscrossed-diagonal cracking of joint panel concrete, yielding of the steel web panel and joint transverse reinforcement, and spalling and crushing of the joint panel concrete. Besides, severe vertical cracks might develop along the inner side of wall boundary element, due to horizontally tensile forces induced by the steel beam flange. Increased amount of horizontally distributed rebar is recommended to be assigned in the join region for controlling such unwanted damage.

(2) The steel beam-to-SRC wall joint using a fully welded connection showed stable hysteretic responses and large deformation capacity. Although failed at beam-to-wall joints, specimens

SRC1 and SRC3 developed an ultimate beam rotation exceeding 5%.

(3) For specimen SRC2 that was capacity designed following the “strong joint-weak coupling beam” mechanism, the damage to the joint was slight and repairable (belonging to damage state DS1 as specified in FEMA P-58) till the steel coupling beam fully developed its plastic rotation of 10%.

(4) A design model was developed to calculate the nominal strength of steel coupling beam-to-SRC wall joints, where the joint panel shear resistance is contributed by the shear mechanism of steel web panel, inner concrete compression strut mechanism and outer concrete compression field mechanism.

(5) The design model of joint strength was examined by collected test data of five specimens and analysis results of 30 refined FE models. The design model provided a reasonable and conservative estimate of the steel beam-to-SRC wall joint strength, with the ratio of FE/experimental-to-calculated values equal to 1.16 on average.

Acknowledgements

The authors gratefully acknowledge sponsorship by Beijing Natural Science Foundation (Grant No. JQ18029) and National Natural Science Foundation of China (Grant No. 51678347). The writers wish to express their sincere gratitude to the sponsors.

References

[1] Harries KA, Mitchell D, Cook WD, Redwood RG. Seismic response of steel beams coupling concrete walls. J Struct Eng 1993; 119(12): 3611-29.

[2] Fortney PJ, Shahrooz BM, Rassati GA. Seismic performance evaluation of coupled core walls with concrete and steel coupling beams. Steel Compos Struct 2007; 7(3): 279-301.

[3] El-Tawil S, Harries KA, Fortney PJ, Shahrooz BM, Kurama Y. Seismic design of hybrid coupled

wall systems: State of the art. J Struct Eng 2010; 136(7): 755-769.

[4] Fortney PJ, Shahrooz BM, Rassati GA. Large-scale testing of a replaceable “fuse” steel coupling beam. J Struct Eng 2007; 133(12): 1801-7.

[5] Ji X, Wang Y, Ma Q, Okazaki T. Cyclic behavior of very short steel shear links. J Struct Eng 2016; 142(2): 04015114.

[6] Ji X, Wang Y, Ma Q, Okazaki T. Cyclic behavior of replaceable steel coupling beams. J Struct Eng 2017; 143(2): 04016169.

[7] Ji X, Liu D, Sun Y, Molina Hutt C. Seismic performance assessment of a hybrid coupled wall system with replaceable steel coupling beams versus traditional RC coupling beams. Earthquake Eng. Struct. D 2017; 46(4): 517-35.

[8] Ji X, Wang Y, Zhang J, Okazaki T. Seismic behavior and fragility curves of replaceable steel coupling beams with slabs. Eng Struct 2017; 150: 622-35.

[9] Qian J, Jiang Z, Ji X. Behavior of steel tube-reinforced concrete composite walls subjected to high axial force and cyclic loading. Eng Struct 2012; 36(3): 173-84.

[10] Ji X, Sun Y, Qian J, Lu X. Seismic behavior and modeling of steel reinforced concrete (SRC) walls. Earthquake Eng. Struct. D 2015; 44(6): 955-72.

[11] Dan D, Fabian A, Stoian V. Theoretical and experimental study on composite steel-concrete shear walls with vertical steel encased profiles. J Struct Constr Eng 2011, 67(5): 800-13.

[12] Massone LM, Sayre BL, Wallace JW. Load-deformation responses of slender structural steel reinforced concrete walls. Eng Struct 2017; 140: 77-88.

[13] Shahrooz BM, Remmetter ME, Qin F. Seismic design and performance of composite coupled walls. J Struct Eng 1993; 119(11): 3291-309.

[14] Park WS, Yun HD. Bearing strength of steel coupling beam connections embedded reinforced concrete shear wall. Eng Struct 2006; 28(9): 1319-34.

[15] AISC. Seismic provisions for structural steel buildings (ANSI/AISC 341-10), Chicago:

American Institute of Steel Construction; 2010.

[16] Song A. Research on seismic performance of connection in innovative hybrid coupled wall system. Ph.D. thesis, Xi'an: Xi'an University of Architecture and Technology, 2014. [in Chinese].

[17] Wu Y, Zhou Z, Xiao Y, Yang W. Experimental study on steel coupling beam and composite shear wall connection under simulated earthquake action. J Build Struct 2015; 36(9): 9-17, 52. [in Chinese].

[18] Li GQ, Gu F, Jiang J, Sun F. Cyclic behavior of steel beam-concrete wall connections with embedded steel columns (I): Experimental study. Steel Compos. Struct 2017; 23(4): 399-408.

[19] Li GQ, Gu F, Jiang J, Sun F. Cyclic behavior of steel beam-concrete wall connections with embedded steel columns (II): Theoretical study. Steel Compos. Struct 2017; 23(4): 409-20.

[20] CMC. Code for seismic design of buildings (GB 50011-2010). Beijing: China Ministry of Construction; 2016.

[21] CMC. Technical Specification for concrete structures of tall building (JGJ 3-2010). Beijing: China Ministry of Construction, 2010. [in Chinese].

[22] CMC. Code for design of concrete structures (GB 50010-2010). Beijing: China Ministry of Construction; 2010. [in Chinese].

[23] Technical Committee ISO/TC 17. International standard of steel for the reinforcement of concrete - part 2 ribbed bars (ISO 6935-2:2015). Geneva: International Standards Organization; 2015.

[24] CMC. Code for design of composite structures (JGJ 138-2016). Beijing: China Ministry of Construction; 2016. [in Chinese].

[25] CMC. Specification of seismic test of buildings (JGJ 101-2015). Beijing: China Ministry of Construction; 2015. [in Chinese].

[26] CMC. Code for design of strengthening concrete structure (GB 50367-2010). Beijing: China Ministry of Construction; 2010. [in Chinese].

[27] Okazaki T, Arce G, Ryu HC, Engelhardt MD. Experimental study of local buckling, overstrength, and fracture of links in eccentrically braced frames. J Struct Eng 2005, 131(10): 1526-35.

[28] ATC. FEMA P-58-1: Seismic performance assessment of buildings. Volume 1 – methodology. Washington, DC: Federal Emergency Management Agency; 2012.

[29] ASCE. Seismic rehabilitation of existing buildings. ASCE/SEI 41–13. Reston, VA: American Society of Civil Engineers; 2014.

[30] Deierlein GG, Sheikh TM, Yura JA, Jirsa JO. Beam-column moment connections for composite frames: Part 2. J Struct Eng 1989, 115(11): 2877-96.

[31] ASCE Task Committee on Design Criteria for Composite Structures in Steel and Concrete. Guideline for design of joints between steel beams and reinforced concrete columns. J Struct Eng 1994;120(8): 2330–51.

[32] ABAQUS. Analysis User's Manual. Version 6.10. USA: ABAQUS Inc., Dassault Systèmes, 2010.

[33] Dusicka P, Itani AM, Buckle IG. Cyclic response of plate steels under large inelastic strains. J Constr Steel Res 2007, 63(2): 156-64.